# NMR Structure and Backbone Dynamics of the Extended Second Transmembrane Domain of the Human Neuronal Glycine Receptor $\alpha_1$ Subunit†

Victor E. Yushmanov,‡ Pravat K. Mandal,‡ Zhanwu Liu,‡ Pei Tang,‡,§ and Yan Xu*,‡,§

*Department of Anesthesiology and Department of Pharmacology, University of Pittsburgh School of Medicine, Pittsburgh, Pennsylvania 15261*

*Received August 30, 2002; Revised Manuscript Received December 20, 2002*

ABSTRACT: The structure and backbone dynamics of an extended second transmembrane segment (TM2e) of the human neuronal glycine receptor $\alpha_1$ subunit in sodium dodecyl sulfate micelles were studied by $^1$H and $^{15}$N solution-state NMR. The 28-amino acid segment contained the consensus TM2 domain plus part of the linker between the second and third transmembrane domains. The presence of a well-structured helical region of at least 13 amino acids long and an unstructured region near the linker was evident from the proton chemical shifts and the pattern of midrange nuclear Overhauser effects (NOE). $^{15}$N relaxation rate constants, $R_1$ and $R_2$, and $^{15}$N-{$^1$H} NOE indicated restricted internal motions in the helical region with NOE values between 0.6 and 0.8. The squared order parameter ($S^2$), the effective correlation time for fast internal motions ($\tau_e$), and the global rotational correlation time ($\tau_m$) were calculated for all TM2e backbone N−H bonds using the model-free approach. The $S^2$ values ranged about 0.75−0.86, and the $\tau_e$ values were below 100 ps for most of the residues in the helical region. The $\tau_m$ value, calculated from the dynamics of the helical region, was 5.1 ns. The $S^2$ values decreased to 0.1, and the $\tau_e$ values sharply increased up to 1.2 ns at the linker near the C-terminus, indicating that the motion of this region is unrestricted. The results suggest a relatively high degree of motional freedom of TM2e in micelles and different propensities of the N- and C-terminal moieties of the transmembrane domain to assume stable helical structures.

Neurotransmitter-gated synaptic ion channels, including the glycine receptor (GlyR),[1] $\gamma$-aminobutyric acid type A ($GABA_A$) receptor, nicotinic acetylcholine receptor, and 5-hydroxytryptamine 5-$HT_3$ receptor, are responsible for the fast synaptic transmission in the central nervous system. They are considered to be the molecular targets for low-affinity neurological agents such as volatile general anesthetics and short-chain alcohols (*1*). The structures of synaptic ion channels belonging to this superfamily are formed by oligomerization of five subunits, each of which contains four transmembrane domains. Site-directed mutagenesis has suggested an inhibitory site within the aqueous pore of nicotinic acetylcholine receptor (*2*) and potentiating sites at the extracellular interfacial regions of transmembrane domains 2 and 3 (TM2 and TM3) of the glycine and $GABA_A$ receptors (*3*). It is believed that the TM2 domains of each receptor subunit line the pore of the channel and thus are the critical transmembrane component for the functional activity of the receptor. Our understanding of their structure and dynamics, and of the gating mechanism, however, remains incomplete.

To obtain structural information of membrane-associated proteins and peptides, micelles of surfactants, e.g., dodecylphosphocholine (DPC) and sodium dodecyl sulfate (SDS), are commonly used to enable the application of high-resolution, solution-state nuclear magnetic resonance (NMR) techniques. The channel-lining TM2 segments of the nicotinic acetylcholine receptor and of the NMDA receptor were studied in DPC micelles and lipid bilayers by solution and solid-state NMR (*4*). It has been demonstrated recently that solubilization of functional TM2 segments of GlyR in surfactant micelles can yield pentameric bundles (*5*), suggesting that the micelles may provide an adequate membrane-mimicking environment for transmembrane channel assembly. It was also shown earlier that the TM2 segments of the human GlyR $\alpha_1$ subunit alone form homopentameric channels with conductance characteristics very similar to those of a natural receptor (*6*, *7*). Hence, the study of isolated functional segments of the putative pore-lining TM2 domains of GlyR in micelles is warranted.

In our previous work, the structure of the TM2 segment (23 amino acids) of human GlyR $\alpha_1$ subunit and its anesthetic-insensitive single-point mutant, S267Y, in SDS and DPC micelles were determined by $^1$H NMR at 600 and

† This work was supported by NIH Grants R01 GM49202 to Y.X. and R01 GM56257 to P.T.

* Send all correspondence to Professor Yan Xu, Ph.D. W-1358 Biomedical Science Tower, University of Pittsburgh School of Medicine, Pittsburgh, PA 15261; (412) 648-9922; Fax (412) 648-9587; xuy@anes.upmc.edu.

‡ Department of Anesthesiology.

§ Department of Pharmacology.

[1] Abbreviations: GlyR, glycine receptor; GABA, $\gamma$-aminobutyric acid; TM2 and TM3, transmembrane domains 2 and 3; DPC, dodecylphosphocholine; SDS, sodium dodecyl sulfate; NMR, nuclear magnetic resonance; $R_1$ and $R_2$, longitudinal and transverse relaxation rate constants, respectively; NOE, nuclear Overhauser effect; TM2e, extended TM2 segment of the human neuronal GlyR $\alpha_1$ subunit; TFE, trifluoroethanol; CD, circular dichroism; SDS−PAGE, sodium dodecyl sulfate−polyacrylamide gel electrophoresis; 2D and 3D, two- and three-dimensional; HSQC, heteronuclear single-quantum coherence; NOESY, NOE spectroscopy; TOCSY, total correlation spectroscopy; $\tau_m$, global rotational correlation time; $\tau_e$, effective correlation time for fast internal motions; $S^2$, squared order parameter.

10.1021/bi026767g CCC: $25.00 
Published on Web 03/14/2003

750 MHz and by circular dichroism (CD) (*5*, *8*). The NMR structures showed right-handed α helices without kinks. A well-defined hydrophilic path along the helical surfaces has been characterized. A model of pore architecture has been suggested based on the side-chain arrangement of the NMR-derived structures and the energy minimization of a homopentameric TM2 channel in a 1,2-dimyristoyl-*sn*-glycero-3-phosphocholine membrane. Our recent results suggest that the channel activity upon interaction with volatile general anesthetics may be more closely related to the peptide dynamics than to its static structure in membrane (*9*, *10*). The dynamics of the GlyR TM2 segment, however, has not been studied.

Protein dynamics is an important factor capable of influencing protein structure, stability, and function (*11*). The longitudinal and transverse relaxation rate constants ($R_1$ and $R_2$) and $^{15}$N-{$^1$H} steady-state nuclear Overhauser effect (NOE) of a given amide $^{15}$N are influenced mainly by dipolar interaction with its attached proton and by $^{15}$N chemical shift anisotropy. The strength of the dipolar interaction is determined by the motion of the N−H bond vector. The backbone dynamics of several uniformly $^{15}$N-labeled membrane peptides and proteins of nonchannel origin, such as bacteriophage coat proteins (*12*−*14*), adrenal peptide E (*15*), bacterial light-harvesting complex (*16*), and preferredoxin transit peptide (*17*), have been studied recently by $^{15}$N magnetic relaxation measurements in micellar environment.

In the present work, we report the structure and backbone dynamics of an extended TM2 chain of the human neuronal GlyR $\alpha_1$ subunit (TM2e) in SDS micelles. The 28-residue TM2e, APARVGLGITTVLTMTTQSSGSRASLPK (molecular mass of 2.8 kDa), contains the fragment between V253 and S270, which has been predicted to be the second transmembrane domain based on the relative hydrophobicity scale (see www.expasy.org). Thus, compared to the predicted TM2 segment, TM2e is extended by four additional residues at the N-terminus and by six at the C-terminus. The latter is part of a putative hinge region between TM2 and TM3. This article addresses the following two issues: (a) the influence of the addition of extra residues on the TM2e folding and (b) the relation of the peptide backbone dynamics to its three-dimensional (3D) structure in the micellar environment.

## MATERIALS AND METHODS

*Protein Expression.* The cDNA for the complete human glycine receptor $\alpha_1$ chain, obtained from Dr. Michael Cascio (University of Pittsburgh), was used as a template for the PCR amplification of the TM2e segment. The plasmid of TM2e segment, encoding amino acids A249−K276, was constructed with BamHI and EcoRI restriction sites (Sigma-Genosys, Woodlands, TX), and ligated into the pGEX-3X vector (Amersham Pharmacia Biotech, Uppsala, Sweden) using the Rapid DNA Ligation kit (Roche Molecular Biochemicals, Mannheim, Germany). The subclones of GST-TM2e were transformed into *Escherichia coli* BL21(DE3)-pLysS competent cells (Novagen, Madison, WI) for protein expression. The expression was induced by adding isopropyl-*β*-D-thiogalactopyranoside to a final concentration of 0.2 mM when OD ($\lambda$600) value reached 0.6−0.8. The induction time was about 2.5 h. For uniform $^{15}$N TM2e labeling, M9 minimal medium was prepared with $(^{15}NH_4)_2SO_4$ as the sole nitrogen source. Standard protocols (Amersham Pharmacia Biotech) for cell lysis, extraction, and purification were followed. The cleavage of TM2e from GST was achieved by Factor Xa enzyme in Glutathione Sepharose 4B columns (Amersham Pharmacia Biotech). The characterization of the product by HPLC and mass spectrometry is presented in Supporting Information. A minor contaminant, originated from earlier termination of the expression at R271, was below 23% of the total peptide amount in the worst batch of samples (see Supporting Information). In the resulting TM2e peptide, the two arginines (R252 and R271) were numbered as R0 and R19, respectively, using the convention suggested by Miller (*18*).

*Sample Preparation.* For reconstitution of the TM2e peptide into SDS micelles, a 2.5 mM TM2e solution in trifluoroethanol (TFE) was dried into thin film under a stream of nitrogen gas, and added with an aqueous solution of SDS-$d_{25}$ to reach a surfactant-to-peptide molar ratio of ∼150. After vigorous mixing, the sample was lyophilized and rehydrated to the final peptide concentration of about 2 mM in water containing 10% $D_2O$ for deuterium lock in NMR measurements. SDS-$d_{25}$ and $D_2O$ were obtained from Cambridge Isotope Laboratories (Andover, MA). SDS-$d_{25}$ was recrystallized from ethanol before use.

*Sodium Dodecyl Sulfate−Polyacrylamide Gel Electrophoresis.* To determine the oligomerization state of TM2e segment in micelle, SDS−PAGE was performed as described by Tatulian and Tamm (*19*). The 12−20% linear gradient gels were used. For electrophoresis, peptide sample was prepared as described above except that the final resuspension was in an aqueous buffer solution containing 0.1 M NaCl and 10 mM Hepes at pH 7.2, followed the addition of the treatment buffer (0.125 M Tris-HCl, 4% SDS, 20% glycerol, 10% *β*-mercaptoethanol, pH 6.8) in a 1:1 volume ratio. Electrophoresis was performed at 20 mA constant current for 1 h using a buffer containing 25 mM Tris, 192 mM glycine, 0.1% SDS (pH 8.3). The gels were stained with Coomassie Blue R-250 (0.1%) for 30 min.

*CD Spectroscopy.* CD spectra in the wavelength range from 185 to 290 nm were obtained at 25 °C on an Aviv CD spectrometer (model 202; Aviv Associates, Lakewood, NJ) with a 1-mm cuvette using a wavelength step of 1 nm, and averaging time of 1 s, and analyzed as described previously (*5*, *19*).

*NMR Spectroscopy.* Two-dimensional (2D) and 3D NMR spectra were recorded at 30 °C on Bruker DRX-500 and Avance-600 NMR spectrometers (Bruker Instruments, Billerica, MA) equipped with triple resonance, triple-axis gradient TXI (500 MHz) or TBI (600 MHz) probes, and operating at 500.13 and 600.83 MHz, respectively, for $^1$H, and at 50.68 and 60.88 MHz, respectively, for $^{15}$N. Typically, the duration of 90° high-power pulses was ∼9 $\mu$s for $^1$H and 36 to 42 $\mu$s for $^{15}$N. $^1$H-$^{15}$N-heteronuclear single quantum correlation (HSQC) spectra were typically acquired into 2048 $t_2$ and 80 $t_1$ points, with spectral width of 12−14 ppm for $^1$H, 24 ppm for $^{15}$N, and 16 transients for each time increment. $^{15}$N-decoupled $^1$H homonuclear 2D NOE spectroscopy (NOESY) and total correlation spectroscopy (TOCSY) data were typically acquired in phase-sensitive (States-TPPI) mode into 2048 $t_2$ and 640 $t_1$ points with spectral width of 10 ppm in each dimension, and 72−80 transients per increment. Mixing time of 60 ms was used for TOCSY, and of 100−180 ms for NOESY. For 3D NOESY−HSQC

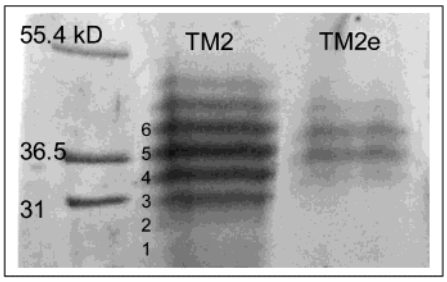


FIGURE 1: SDS−PAGE showing multiple oligomeric forms of TM2e. Left lane: molecular mass standards. The synthetic TM2 segment containing 23 amino acids (*5*) is also shown for comparison.

(mixing time of 150 ms), data matrix consisted of 2048 × 200 × 38 points. For suppression of the solvent peak, the WATERGATE pulse scheme was applied. Spin−lattice ($R_1$) and spin−spin ($R_2$) $^{15}$N relaxation rate constants, and $^{15}$N-{$^1$H} NOE values were repeatedly measured three times for each of the amide nitrogen using standard pulse sequences (*20*) with Echo-Antiecho gradient selection. In relaxation measurements, 120 $t_1$ data points were used with intervals of 2 s between scans and with 12 variable delays ranging from 10 to 1800 ms for $R_1$, and between 20 and 600 ms for $R_2$. In NOE experiments, 360 indirect data points were acquired with or without proton saturation in interleaved fashion. Saturation was achieved by a train of 120° pulses at 5-ms intervals for 3 s.

*Data Processing and Analysis.* Data were processed using NMRPipe and NMRDraw (*21*) and analyzed using PIPP (*22*) and Sparky (*23*) software. For structure calculations, distance restraints, derived from NOESY experiments, were grouped into four categories, i.e., <2.8 Å for strong NOEs, <3.3 Å for medium, <5.0 Å for weak, and <6.0 Å for very weak NOEs (*24*). The initial structure calculations were done using NOE constraints with the simulated annealing protocol (*25*) in X-PLOR (*26*). Structures with no violations above the threshold conditions of 5° for angle, improper, and dihedral angles, and 0.05 and 0.5 Å for bonds and NOEs, respectively, were taken for further refinement. For residues showing $d_{\alpha N}$(i,i+3) and $d_{\alpha\beta}$(i,i+3) NOE connectivities, hydrogen bond constraints of CO(i) to NH(i+4) were included in the refinement. Each hydrogen bond was converted into two distance restraints $r_{NH-O}$ (1.7−1.9 Å) and $r_{N-O}$ (2.3−2.8 Å) (*27*, *28*). Thirty lowest energy structures were used for the refinement. In dynamic studies, $^{15}$N $R_1$ and $R_2$ values were determined from two-parameter fits of peak intensities vs variable delay to a single-exponential function. $^{15}$N-{$^1$H} NOE values are reported as peak intensity ratios obtained with and without $^1$H saturation. The global tumbling time ($\tau_m$) was first estimated from the $R_2/R_1$ ratio (*29*). The squared order parameter ($S^2$), the effective correlation time for fast internal motions ($\tau_e$), and the refined $\tau_m$ value were obtained by fitting the $R_1$, $R_2$, and NOE values in the framework of Lipari-Szabo formalism (*30*, *31*) using the Modelfree software package (*32*, *33*).

## RESULTS

*Structure of TM2e.* Similar to the previously studied TM2 segment composed of 23 amino acids, TM2e was shown to aggregate into oligomers in the micellar environment, with the tetramers and pentamers being predominant (Figure 1). $^{15}$N-$^1$H HSQC NMR spectrum of backbone NH region of

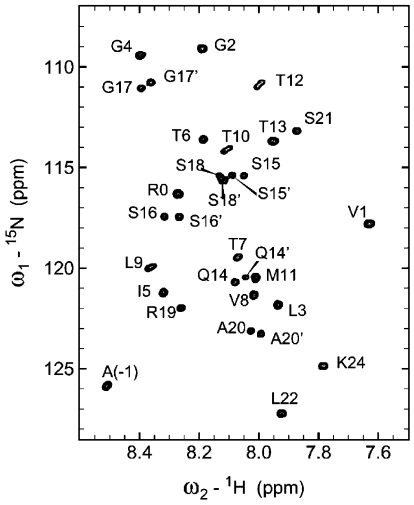


FIGURE 2: Assigned amide backbone region of a $^1$H-$^{15}$N-HSQC NMR spectrum of 2.0 mM TM2e of GlyR in aqueous micelles of SDS-$d_{25}$ at 30 °C. For the residues where peak doubling exists, additional peaks are marked by a prime sign.

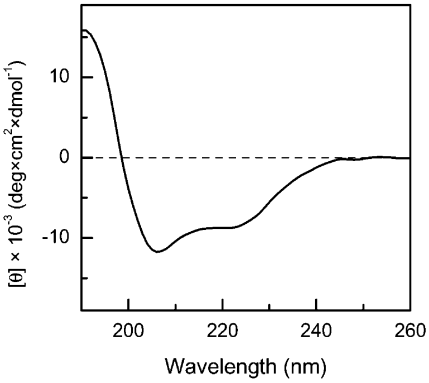


FIGURE 3: Far-UV CD spectrum of the human glycine receptor TM2e fragment in aqueous micelles of SDS at 25 °C.

TM2e in SDS is presented in Figure 2. The peaks for all individual amino acids are well resolved and have been identified (except for proline and N-terminal alanine). In addition, apparent peak doublings for Q14, S15, S16, G17, S18, and A20 were observed, with the maximum doubling for S16 in $^1$H dimension and for G17 in $^{15}$N dimension. Peak shapes of L9, T10, and T12 also show some poorly resolved doubling. To gain an insight into the nature of the peak doubling, variable temperature experiments were performed in the range of 25−40 °C. Peak separation showed a negative temperature coefficient in the $^1$H dimension for Q14, S15, S16, and G17, and a positive coefficient for A20 (up to 0.4 Hz/°C at 600 MHz in the temperature range studied).

Homonuclear 2D TOCSY and 3D NOESY−HSQC experiments allowed the complete $^1$H and $^{15}$N peak assignment for TM2e in SDS (see Supporting Information). Both CD spectra (Figure 3) and NMR spectra of the TM2e in SDS micelles showed the presence of helical secondary structure. Using the molar ellipticity value at 222 nm, CD spectra yielded an estimated helical component of 20−30%. In NOESY spectra, the interresidue cross-peaks were readily detectable, but only through the chain of nonprimed peaks (in Figure 2), and no NOEs were detected between the primed and nonprimed peaks. No intermonomer NOEs were observed in oligomeric bundles, presumably due to the rapid

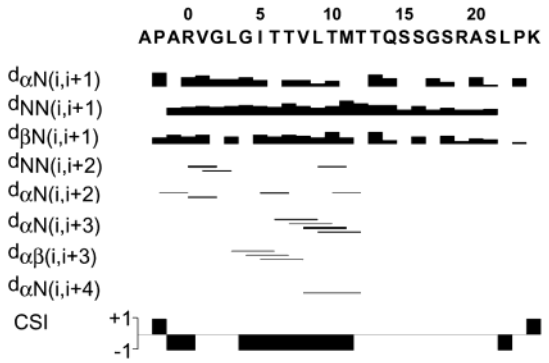


FIGURE 4: Summary of NOE connectivities in the human glycine receptor TM2e fragment in SDS micelles. Sequential and midrange NOE connectivities are presented; the widths of the lines are related to the observed NOE intensities. A preliminary identification of the helical secondary structure based on the chemical shift index (CSI) for $H^{\alpha}$ protons (*34*) is shown at the bottom.

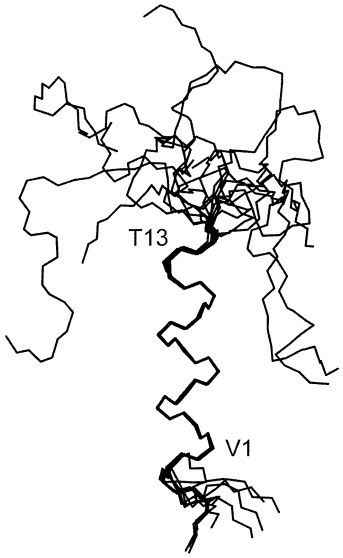


FIGURE 5: Structure of TM2e in SDS micelles. Backbone traces of the 10 lowest energy structures (C-terminus up). A helical structure in the region closer to the N-terminus and a relatively large nonstructured fragment at the C-terminal side can be identified.

relative motion of the monomers. Midrange $H^{\alpha}_{i}$-$H^{N}_{i+3}$, $H^{\alpha}_{i}$-$H^{\beta}_{i+3}$, and $H^{\alpha}_{i}$-$H^{N}_{i+4}$ NOEs are summarized in Figure 4. The NOE connectivities, characteristic of the helix, together with the chemical shift index (based on deviations of $H^{\alpha}$ proton chemical shifts from their random-coil values (*34*)), provided a preliminary identification of the secondary structure. The structures of TM2e in SDS calculated using the NOE restrains are shown in Figure 5.

*Backbone Dynamics of TM2e.* The results of $R_1$, $R_2$, and NOE measurements for TM2e in SDS are given in Figure 6. For most residues (except for those close to the C-terminus), the $R_1$ and $R_2$ values were in the ranges of 1.5−1.9 $s^{-1}$, and 5.0−7.9 $s^{-1}$, respectively. NOE values were above 0.6 for residues between G4 and M11, decreasing at both termini. Negative NOEs were found for three amino acids in the C-terminus but not in the N-terminus. This decline in NOE in the C-terminal region of TM2e was accompanied by a downward trend in both $R_1$ and $R_2$ in the same region of TM2e. For the residues between Q14 and A20, most of the $R_1$, $R_2$, and NOE values are smaller for the primed peaks in Figure 2 than for the nonprimed peaks (Figure 6).

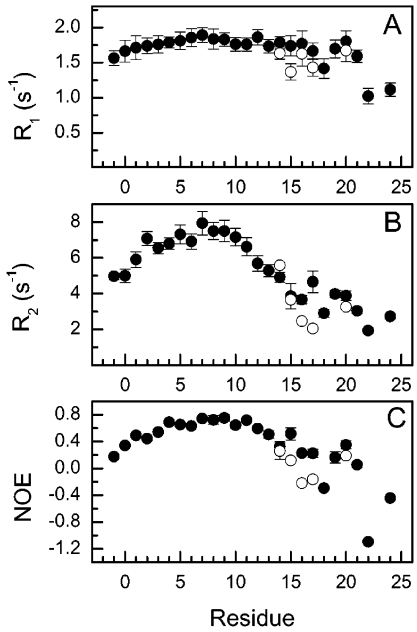


FIGURE 6: (A) Backbone amide $^{15}N$ NMR longitudinal ($R_1$) and (B) transverse ($R_2$) relaxation rate constants and (C) $^{15}N$-{$^1H$} steady-state NOE for TM2e in SDS micelles at magnetic field strength corresponding to a $^1H$ Larmor frequency of 600 MHz at 30 °C. The values for extra peaks (indicated by prime signs in Figure 2) are given by open symbols. Where the error bars are absent, the errors are smaller than the size of the symbol.

The dynamics parameters $S^2$, $\tau_e$, and $\tau_m$ were calculated for the backbone N−H bonds of each residue, using the Lipari-Szabo model-free approach and the axially symmetric anisotropic diffusion model. The $R_2/R_1$ ratio for those residues, whose relaxation is not affected by the fast internal motions on the picosecond time scale, is approximately independent of the internal motion and provides an initial estimation for the reorientation time of each NH vector with global tumbling, i.e., the $\tau_m$ of the peptide (*35*). For this purpose, the residues with the $R_2/R_1$ ratio falling outside one standard deviation of the mean, as well as the residues with NOE < 0.65 (a commonly accepted threshold at 600 MHz for $^1H$ (*36*)) were disregarded. The $\tau_m$ value for TM2e was estimated to be approximately 5.5 ns and further refined to 5.1 ns using the model-free formalism.

For the residues between V1 and T13, the $S^2$ values were about 0.75−0.86, and the $\tau_e$ values were typically below 100 ps except for a few with large standard errors (Figure 7). As is usually the case in proteins and peptides with secondary structure, the $S^2$ values decreased, and the $\tau_e$ values sharply increased to hundreds of picoseconds and to as large as ∼1.2 ns at the termini of TM2e. High mobility (i.e., low $S^2$ and high $\tau_e$ values) was observed for a significant portion of the peptide (about one-third) adjacent to the C-terminus.

## DISCUSSION

In the present work, we determined the structure and backbone dynamics of TM2e in SDS micelles. The data indicate the presence of a helical structure with restricted internal motions closer to the N-terminus, and a freely moving random coil fragment at the C-terminus. Relatively high NOE values (Figure 6C) observed for the residues between V1 and T13 are in agreement with the presence of a highly organized secondary structure. We observed a

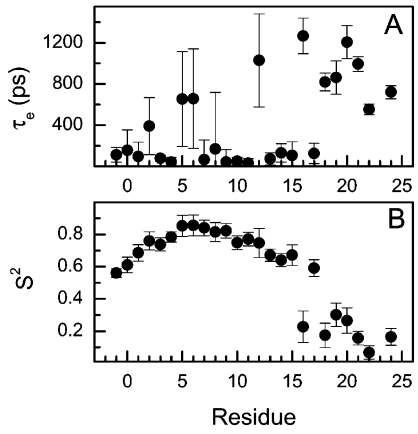


FIGURE 7: (A) The squared order parameter, $S^2$, of N−H bond in TM2e, derived from $^{15}$N amide relaxation measurements in SDS at 30 °C. (B) The corresponding effective correlation time $\tau_e$ for fast internal motions.

significant decrease in the $R_1$, $R_2$, and NOE values in the C-terminal region of TM2e in SDS (Figure 6). This pattern of decrease in $R_1$, $R_2$, and NOE at the ends of the peptide chain is commonly observed for different peptides and proteins in solution (see, for example, refs *36*−*38*) and in micellar environment (*12*−*14*, *16*, *17*). Significant reductions in NOE values compared with the average values for the protein are generally considered as a sign of appreciable internal motions on the picosecond to nanosecond time scales (*35*, *38*).

The decline in NOE values and the observation of negative NOEs for the TM2e residues between G17 and K24 in SDS indicates the significantly increased molecular mobility for this segment of the peptide in micellar preparation. This observation is in agreement with the proposed structure (Figure 5), in which the helix does not extend beyond T13. Indeed, the $H^{\alpha}_{i}$-$H^{N}_{i+3}$ and $H^{\alpha}_{i}$-$H^{\beta}_{i+3}$ NOEs, which are characteristic of helices, were observed only between the residues from L3 to T12. Thus, the C-terminal region of TM2e, i.e., the region beyond its predicted transmembrane domain (V1 to S18), may be located outside the micelle in the form of a random coil in our preparation.

To characterize peptide dynamics, three parameters were derived from the $^{15}$N relaxation measurements: $S^2$, which ranges between 0 and 1 and accounts for the degree of spatial restriction for a backbone amide $^{15}$N-$^{1}$H$^{N}$ bond vector, $\tau_m$, and $\tau_e$ ($\tau_e \ll \tau_m$) (*30*, *31*). The dynamics parameters given in Figure 7 show that for the residues between V1 and T13, where the $S^2$ values were above 0.65 and the $\tau_e$ values were mostly below 100 ps, rapid internal motions are restricted. In contrast, for the residues at the N-terminus and especially at and near the C-terminus, a much smaller order parameter and much higher $\tau_e$ values were observed, characteristics of the absence of well-defined secondary structure.

Determination of the backbone dynamics parameters from amide $^{15}$N NMR relaxation measurements requires certain methodological considerations. The $\tau_m$ values are generally expected to be significantly larger in micelles than in solution due to slower tumbling of the whole peptide−micelle complex. The $\tau_m$ value obtained for TM2e in SDS (5.1 ns), however, is smaller than the corresponding values (8−20 ns) for peptides of comparable size in micelles obtained by similar $^{15}$N relaxation measurements as reported by others (*12*−*16*). Every precaution was taken in repeated measurements to rule out any experimental inaccuracies in the transverse relaxation experiments, such as sample heating or CPMG pulse train imperfections. A potential bias in using $R_2$ for $\tau_m$ determination may cause systematic overestimation rather than underestimation of $\tau_m$ (*39*). Other explanations of the discrepancy may be found in the peculiarities of the peptide dynamics. Estimating $\tau_m$ based on the $R_2/R_1$ ratio assumes that the tumbling is isotropic and that the internal motions are independent of the $\tau_m$ tumbling. If this were the case, and the peptide were rigidly bound to the micelle, then $\tau_m$ would be around 11.5 ns, according to the molecular mass of the peptide−micelle complex (approximately 0.5 ns per kDa for isotropic tumbling). However, in the presence of a rigid peptide of comparable or larger linear dimensions, micelle is no longer a normal spherical micelle (*40*). Moreover, the apparent $\tau_m$ may be increased by conformation and solvent exchange processes (*41*). Some of the authors reporting anomalously large global correlation times of 16−20 ns explain their and similar results by high sample or electrolyte concentration, and by intermediate chemical exchange between a set of similar conformations (*15*). Alternatively, the apparent $\tau_m$ may be reduced by internal motions on the nanosecond time scale involving significant portion of the protein (*42*).

In our case, considering the relatively short helical part of TM2e in SDS and quite moderate NOE and $R_2$ values even in its core, it seems probable that the helical element can be flexible enough, resulting in underestimation of apparent $\tau_m$ because of subnanosecond internal motions and some degree of peptide mobility relative to the micelle (*9*). The observation of $\tau_e$ values in subnanosecond to nanosecond range for significant portion of the peptide (Figure 7A) may be taken as the evidence for the influence of slower internal motions on $\tau_m$. Although the calculation of $\tau_e$ may not be always reliable (*32*), this finding supports the explanation of the relatively low apparent $\tau_m$ by the presence of such motions. Indeed, it is not unusual to find membrane-bound helices with an increased mobility. In earlier studies of bacteriophage coat proteins in SDS, the presence of two membrane-associated helices with different motional characteristics has been demonstrated (*12*, *13*). For the residues belonging to the more mobile helix in the coat proteins, typical $R_2$ and NOE values were almost identical to the values reported in the present work for the helical region of TM2e (*12*, *13*).

From the discussion above, it is clear that although the absolute values of the dynamics parameters might be influenced by uncertainties in the determination of $\tau_m$, these uncertainties do not change the overall pattern of the principal structural and dynamical features of TM2e. Our tentative simulations of model-free parameters using $\tau_m$ values of up to 10.4 ns (data not shown) also indicated the presence of a region with restricted internal motions, and a freely moving fragment at the C-terminus.

As shown in Figure 2, doubling of several peaks in HSQC spectra was detected for the TM2e peptide in SDS. Although mass spectroscopy did reveal some heterogeneity of TM2e preparation due to earlier termination of the expression, the impurity never exceeded ~23% in the worst batch of samples after reverse-phase HPLC purification (see Supporting Information). This level of contamination does not explain

the observed peak doubling, with the two resonances for a single amide site having similar intensities. Peak doubling with slow (on the NMR time scale) exchange between the species in equilibrium is not uncommon in micelles (*14*, *43*, *44*) and even in solvent mixtures (*45*) as a result of the stabilization of some tentative intramolecular hydrogen bonds in different conformations (*37*) or due to asymmetry in homooligomers (*46*). Our observation may be attributable to two different conformational variations of TM2e. The data in Figure 1 lend substance to the possible interpretation of TM2e peak doubling in terms of the coexistence of oligomers of different order, predominantly tetramers and pentamers, although some asymmetry in oligomers cannot be ruled out either. The two putative conformational variations in SDS are very close, suggesting that micellar environment does not favor wide variety of conformations of the TM2e peptide. A negative temperature coefficient of the $^1$H peak separation in the range of 25−40 °C for doubled peaks (except for A20) suggests that the peaks for the residues closer to the center of TM2e (i.e., Q14, S15, S16, and G17) would merge with increased exchange rate at a higher temperature.

An alternative explanation of peak doubling in SDS might be an inadequate amount of detergent in the sample (*47*). However, the concentration of 300 mM SDS used in our experiments is relatively high as compared to most of similar studies. An attempt to increase SDS concentration was unsuccessful because of poor sample stability above 450 mM SDS (formation of gel and precipitation) (*48*). In contrast to the observations by McDonnell et al. (*47*), we found that the two peaks in each pair were of roughly equal intensity. Moreover, in TFE-$d_2$ (i.e., in the absence of any surfactants), NMR spectra of TM2e also revealed peak doubling for amino acids between L9 and R19, instead of between Q14 and A20 as in SDS (unpublished observation). Therefore, the two conformations may be attributed to the propensity of the TM2e peptide itself to form a variety of conformations rather than to inhomogeneity in micelle structure (e.g., sphere and rod shape equilibrium).

It is reasonable to expect that not the entire peptide is buried inside the micelle. More flexible, probably nonhelical region formed by the residues from Q14 to A20 may be located at the micelle−water interface, the region where the NMR spectra revealed the appearance of the two conformational variations with different peak positions. $^{15}$N relaxation measurements (Figure 6) showed lower $R_1$, $R_2$, and NOE values for observable resonances near the C-terminus (S15−A20) for the conformer marked by prime signs in Figure 2. This, as well as the absence of detectable NOE connectivities for the primed conformer, indicates that the extra conformer is significantly less restricted and more flexible in the interfacial region, as compared to the regular (nonprimed) conformer. The residues near the C-terminus, roughly between S21 and K24, may form a loose random coil in aqueous phase outside the micelle. Fast molecular movements in this region may render different conformers indistinguishable accounting for the single set of peaks for S21−K24.

Similar dynamic behavior was found for TM2e in organic solvent (TFE), namely, the presence of a helical region (more extensive than in SDS) with restricted motions, intermediate region with two distinctly different conformers (one of them showing lower $R_2$ and NOE values), and a freely moving random coil fragment at the C-terminus (unpublished observation). This leads to the conclusion that the principal structural and dynamical features of TM2e in different membrane-mimetic media are determined mainly by the properties of the TM2e itself.

In the present study, the extended hydrophilic C-terminal region enabled better solubilization of TM2e in aqueous SDS micelles. The structure and dynamics of TM2e in SDS may be compared with our previous NMR structural data for a shorter (23 amino acids) TM2 chain of the human neuronal GlyR $\alpha_1$ subunit (*5*) that does not contain the extended unstructured C-terminal region. The $^1$H chemical shifts of the two peptides in SDS were within $<0.1$ ppm of each other for $H^\alpha$ and HN protons of most residues. Both TM2 and TM2e contain a helical structure in the N-terminal half, suggesting that the presence or absence of the extended C-terminal domain does not result in profound structural changes in the major portion of the TM2 region that is involved in the lining of the GlyR ion channel. Recent data on transepithelial ion transport have also shown that the residues involved in the membrane assembly of the TM2 channel pore are apparently located in the N-terminal half of the sequence, and that removing the first five C-terminal residues has minimal effect on the channel conductance (*49*). For the shorter, 23-residue TM2 chain, however, an α-helical pattern was identified from V1 to S16 (*5*), three residues more extended than in TM2e. Some degree of destabilization of secondary structure, as well as a relatively high mobility (and, hence, low $R_2$ values) of the helical fragment as compared to most transmembrane proteins, may be accounted for by the effects of the loose (possibly extramicellar) tail of the longer chain TM2e. Our preliminary studies show that the destabilizing effect is less pronounced in the TM2−TM3 construct once the extended C-terminus is linked to the TM3 domain (unpublished observation). Although this finding underscores the importance of the selection of domain boundaries for subcloning when studying isolated protein fragments in the reductionist approach to structural determination (*50*), the structural and dynamical results of the truncated TM2e are nevertheless significant because they show the propensity of segment Q14−S16 to be flexible.

The S15 residue, which is critical for the modulation of GlyR by alcohols and volatile anesthetics (*3*), is located in the flexible region separating the rigid helical structure and the highly dynamic hinge fragment. With the reservation that care should be taken when transferring the results from an isolated peptide to the native protein, the location of S15 may be discussed in the context of the idea that the peptide dynamics rather than its static structure may determine the membrane channel activity upon interaction with volatile general anesthetics (*9*, *10*). Residues that are located at the borders of highly structured functional units and, therefore, possess higher potential for changes in mobility than those involved into well-structured domains may be responsible for allosteric linkage between ligand binding and channel gating in the membrane-receptor−ligand complexes, and act as molecular "switches" of the ion transport activity. The pore architecture model proposed based on the 23-residue TM2 and large-scale computer simulation (*5*) also suggests the critical involvement of residues in this border region in channel gating.

## ACKNOWLEDGMENT

We are grateful to Professor Michael Cascio for providing cDNA of glycine receptor and Professor Arthur G. Palmer for providing software packages for the analysis of NMR dynamics. We thank Dr. Jian Hu, Ms. Ying Huang, and Ms. Martha Zegarra for technical support in protein expression and purification, and Ms. Martha Zegarra for participation in data processing. We also thank Mr. Virgil Simplaceanu and Professor Chien Ho for arranging the use of the 500 MHz NMR spectrometer.

## SUPPORTING INFORMATION AVAILABLE

HPLC and mass spectra of TM2e. $^{1}H$ and $^{15}N$ peak assignments for TM2e in SDS micelles. This material is available free of charge via the Internet at http://pubs.acs.org.

## REFERENCES

1. Franks, N. P., and Lieb, W. R. (1996) *J. Clin. Anesth. 8*, 3S−7S.
2. Forman, S. A., Miller, K. W., and Yellen, G. (1995) *Mol. Pharmacol. 48*, 574−581.
3. Mihic, S. J., Ye, Q., Wick, M. J., Koltchine, V. V., Krasowski, M. D., Finn, S. E., Mascia, M. P., Valenzuela, C. F., Hanson, K. K., Greenblatt, E. P., Harris, R. A., and Harrison, N. L. (1997) *Nature 389*, 385−389.
4. Opella, S. J., Marassi, F. M., Gesell, J. J., Valente, A. P., Kim, Y., Oblatt-Montal, M., and Montal, M. (1999) *Nat. Struct. Biol. 6*, 374−379.
5. Tang, P., Mandal, P. K., and Xu, Y. (2002) *Biophys. J. 83*, 252−262.
6. Marsh, D. (1996) *Biochem. J. 315*, 345−361.
7. Reddy, G. L., Iwamoto, T., Tomich, J. M., and Montal, M. (1993) *J. Biol. Chem. 268*, 14608−14615.
8. Xu, Y., Tang, P., Zubrzycki, I. Z., and Hu, J. (2000) in *Progress in Anesthetic Mechanism* (Ogli, K., Ed.) pp 306−311, Research Group of Anesthetic Mechanism in Japan, Kagawa.
9. Tang, P., and Xu, Y. (2002) *Proc. Natl. Acad. Sci. U.S.A. 99*, 16035−16040.
10. Tang, P., Mandal, P. K., and Zegarra, M. (2002) *Biophys. J. 83*, 1413−1420.
11. Wand, A. J. (2001) *Nat. Struct. Biol. 8*, 926−931.
12. Almeida, F. C., and Opella, S. J. (1997) *J. Mol. Biol. 270*, 481−495.
13. Papavoine, C. H., Remerowski, M. L., Horstink, L. M., Konings, R. N., Hilbers, C. W., and van de Ven, F. J. (1997) *Biochemistry 36*, 4015−4026.
14. Williams, K. A., Farrow, N. A., Deber, C. M., and Kay, L. E. (1996) *Biochemistry 35*, 5145−5157.
15. Yan, C., Digate, R. J., and Guiles, R. D. (1999) *Biopolymers 49*, 55−70.
16. Sorgen, P. L., Cahill, S. M., Krueger-Koplin, R. D., Krueger-Koplin, S. T., Schenck, C. C., and Girvin, M. E. (2002) *Biochemistry 41*, 31−41.
17. Wienk, H. L., Wechselberger, R. W., Czisch, M., and de Kruijff, B. (2000) *Biochemistry 39*, 8219−8227.
18. Miller, C. (1989) *Neuron 2*, 1195−1205.
19. Tatulian, S. A., and Tamm, L. K. (2000) *Biochemistry 39*, 496−507.
20. Farrow, N. A., Muhandiram, R., Singer, A. U., Pascal, S. M., Kay, C. M., Gish, G., Shoelson, S. E., Pawson, T., Forman-Kay, J. D., and Kay, L. E. (1994) *Biochemistry 33*, 5984−6003.
21. Delaglio, F., Grzesiek, S., Vuister, G. W., Zhu, G., J., P., and Bax, A. (1995) *J. Biomol. NMR 6*, 277−293.
22. Garrett, D. S., Powers, R., Gronenborn, A. M., and Clore, G. M. (1991) *J. Magn. Reson. 95*, 214−220.
23. Goddard, T. D., and Kneller, D. G. *SPARKY 3*, University of California, San Francisco.
24. Cai, M., Huang, Y., Zheng, R., Wei, S. Q., Ghirlando, R., Lee, M. S., Craigie, R., Gronenborn, A. M., and Clore, G. M. (1998) *Nat. Struct. Biol. 5*, 903−909.
25. Nilges, M., Clore, G. M., and Gronenborn, A. M. (1988) *FEBS Lett. 229*, 317−324.
26. Brünger, A. T. (1992) *X-PLOR: A System for X-ray Crystallography and NMR. Version 3.581*, Yale University Press, New Haven, CT.
27. Baker, E. N., and Hubbard, R. E. (1984) *Prog. Biophys. Mol. Biol. 44*, 97−179.
28. Mitchell, J. B. O., and Price, S. L. (1990) *J. Comput. Chem. 11*, 1217−1233.
29. Kay, L. E., Torchia, D. A., and Bax, A. (1989) *Biochemistry 28*, 8972−8979.
30. Lipari, G., and Szabo, A. (1982) *J. Am. Chem. Soc. 104*, 4546−4559.
31. Lipari, G., and Szabo, A. (1982) *J. Am. Chem. Soc. 104*, 4559−4570.
32. Palmer, A. G., III, Rance, M., and Wright, P. E. (1991) *J. Am. Chem. Soc. 113*, 4371−4380.
33. Mandel, A. M., Akke, M., and Palmer, A. G., III. (1995) *J. Mol. Biol. 246*, 144−163.
34. Wishart, D. S., Sykes, B. D., and Richards, F. M. (1992) *Biochemistry 31*, 1647−1651.
35. Lee, L. K., Rance, M., Chazin, W. J., and Palmer, A. G., III. (1997) *J. Biomol. NMR 9*, 287−298.
36. Mercier, P., Spyracopoulos, L., and Sykes, B. D. (2001) *Biochemistry 40*, 10063−10077.
37. Orekhov, V. Y., Korzhnev, D. M., Diercks, T., Kessler, H., and Arseniev, A. S. (1999) *J. Biomol. NMR 14*, 345−356.
38. Jia, X., Lee, L. K., Light, J., Palmer, A. G., III, and Assa-Munt, N. (1999) *J. Mol. Biol. 292*, 1083−1093.
39. Lee, A. L., and Wand, A. J. (1999) *J. Biomol. NMR 13*, 101−112.
40. Papavoine, C. H., Konings, R. N., Hilbers, C. W., and van de Ven, F. J. (1994) *Biochemistry 33*, 12990−12997.
41. Tjandra, N., Feller, S. E., Pastor, R. W., and Bax, A. (1995) *J. Am. Chem. Soc. 117*, 12562−12566.
42. Korzhnev, D. M., Orekhov, V. Y., and Arseniev, A. S. (1997) *J. Magn. Reson. 127*, 184−191.
43. Fernandez, C., Hilty, C., Bonjour, S., Adeishvili, K., Pervushin, K., and Wuthrich, K. (2001) *FEBS Lett. 504*, 173−178.
44. Arora, A., Abildgaard, F., Bushweller, J. H., and Tamm, L. K. (2001) *Nat. Struct. Biol. 8*, 334−338.
45. Abdul-Manan, N., and Hinton, J. F. (1994) *Biochemistry 33*, 6773−6783.
46. Nooren, I. M. A., Kaptein, R., Sauer, R. T., and Boelens, R. (1999) *Nat. Struct. Biol. 6*, 755−759.
47. McDonnell, P. A., Shon, K., Kim, Y., and Opella, S. J. (1993) *J. Mol. Biol. 233*, 447−463.
48. Damberg, P., Jarvet, J., and Graslund, A. (2001) *Methods Enzymol. 339*, 271−285.
49. Broughman, J. R., Shank, L. P., Takeguchi, W., Schultz, B. D., Iwamoto, T., Mitchell, K. E., and Tomich, J. M. (2002) *Biochemistry 41*, 7350−7358.
50. Bagby, S., Tong, K. I., and Ikura, M. (2001) *Methods Enzymol. 339*, 20−41.

BI026767G